AGU PUBLICATIONS

Geophysical Research Letters

RESEARCH LETTER
10.1002/2014GL059683

Key Points:
- Electron temperatures at the main ionospheric peak are independent of SZA
- This explains observed peak density-SZA relationship
- Dependence of electron temperature on several factors is predicted

Correspondence to:
P. Withers,
withers@bu.edu

Citation:
Withers, P., K. Fallows, and M. Matta (2014), Predictions of electron temperatures in the Mars ionosphere and their effects on electron densities, *Geophys. Res. Lett.*, *41*, 2681–2686, doi:10.1002/2014GL059683.

Received 20 FEB 2014
Accepted 26 MAR 2014
Accepted article online 31 MAR 2014
Published online 22 APR 2014

Predictions of electron temperatures in the Mars ionosphere and their effects on electron densities

Paul Withers[1,2], Kathryn Fallows[1], and Majd Matta[2]

[1]Department of Astronomy, Boston University, Boston, Massachusetts, USA, [2]Center for Space Physics, Boston University, Boston, Massachusetts, USA

Abstract Observations of peak electron densities in the Mars ionosphere are well fit by a simplistic theory that assumes the electron temperature, T_e, at the peak remains constant as solar zenith angle, χ, changes. However, T_e ought to vary with both altitude and χ. Here we use an existing numerical model of ionospheric energetics, which includes both vertical and diurnal variations in temperatures, to predict that T_e at the ionospheric peak is relatively independent of χ. This model accurately predicts the observed dependence of peak electron density on χ, whereas predictions using Viking-based electron temperatures that are held constant with time do not. A simplified analytic model is developed to interpret these results further. It predicts that the difference between electron and neutral temperatures is proportional to the ratio of electron heating rate to electron production rate and proportional to the square root of solar irradiance.

1. Introduction

The production of ionospheric plasma in most solar system ionospheres is controlled by solar photoionization. Consequently, the dependence of plasma density on solar zenith angle is a useful indicator of ionospheric processes. Many investigations of observed peak electron densities in the ionosphere of Mars have concluded that peak density, N_m, is proportional to the cosine of solar zenith angle, χ, raised to the power k, where $k = 0.5$ [*Hantsch and Bauer*, 1990; *Fox and Yeager*, 2006; *Nielsen et al.*, 2006; *Safaeinili et al.*, 2007; *Gurnett et al.*, 2008; *Morgan et al.*, 2008; *Fox and Yeager*, 2009; *Němec et al.*, 2011]. Indeed, an exponent k of 0.5 is predicted by the simplest possible ionospheric model [*Chapman*, 1931a, 1931b]. In such a Chapman model, $N_m^2 = F/(\alpha eH\mathrm{Ch}(\chi))$, where F is the ionizing flux, α is the rate coefficient for dissociative recombination of molecular ions, $e = \exp(1)$, H is the neutral scale height, and Ch is a geometrical correction factor that reduces to sec χ for small solar zenith angles [*Withers*, 2009]. However, the dissociative recombination coefficient for O_2^+, the dominant ion at the peak of the Mars ionosphere, is a function of electron temperature, T_e [*Schunk and Nagy*, 2009]. Electron temperatures generally increase with altitude in a planetary ionosphere [*Bauer and Lammer*, 2004; *Schunk and Nagy*, 2009]. This ensures that electron thermal energy is conducted downward into the dense neutral atmosphere, where it can be most effectively transferred to cooler neutral molecules. Also, electron temperatures generally decrease with increasing solar zenith angle in a planetary ionosphere as solar heating weakens [*Bauer and Lammer*, 2004; *Schunk and Nagy*, 2009]. Meanwhile, the ionospheric peak is not fixed in altitude: it rises upward as solar zenith angle increases, approximately tracking the level at which the optical path length of sunlight at ionizing wavelengths is unity. Consequently, variations in electron temperature at the ionospheric peak with solar zenith angle ought to modify the dependence of electron density on solar zenith angle from that expected under idealized isothermal conditions. Hence, the exponent k will not equal 0.5. It is not intuitively obvious whether the electron temperature at the ionospheric peak should increase or decrease with increasing solar zenith angle, and there is no a priori reason to expect it to be independent of solar zenith angle, which prompts a question: why is the observed exponent k of 0.5?

Motivated by that question, here we explore how changes in electron temperature with solar zenith angle and altitude affect the dependence of peak electron density on solar zenith angle. We also investigate which factors have the greatest effect on electron temperatures and whether electron temperature measurements can be converted directly into estimates of electron heating rates. We use numerical simulations to test the possibility that the electron temperature at the ionospheric peak is independent of solar zenith angle, and we develop and apply analytic models to gain insight into the functional dependencies that control electron temperatures. It is interesting to note that at Titan, whose ionosphere is somewhat similar to Mars's

ionosphere, electron temperatures at the ionospheric peak appear to be independent of solar zenith angle [*Ågren et al.*, 2009], but we postpone further investigation of this comparative planetology approach for future work.

Section 2 describes previous observations and simulations of how electron temperatures at Mars depend on altitude and solar zenith angle. It also uses an existing numerical model to simulate how electron temperatures at the ionospheric peak vary with solar zenith angle and considers how these results affect the value of the exponent k discussed above. Section 3 identifies the key physical processes controlling electron temperatures near the ionospheric peak and develops an analytic model of how they depend on altitude and solar zenith angle. It also shows how observed electron temperatures can provide an estimate of electron heating rates. Section 4 discusses our results and conclusions.

2. Electron Temperatures at Mars

Electron temperatures at the ionospheric peak and their variation with solar zenith angle have not been constrained by direct observations. The electron temperature profile obtained from the Viking Lander 1 retarding potential analyzer at a solar zenith angle of 40° is the only electron temperature profile ever measured at Mars, and it does not extend to low enough altitudes to encompass the ionospheric peak [*Hanson and Mantas*, 1988]. Models that reproduce the Viking Lander high-altitude electron temperature measurements predict that T_e increases by hundreds of Kelvin from 120 km, the subsolar peak altitude, to 150 km, the near-terminator peak altitude [*Chen et al.*, 1978; *Johnson*, 1978; *Rohrbaugh et al.*, 1979; *Cravens et al.*, 1980; *Singhal and Whitten*, 1988; *Choi et al.*, 1998; *Matta et al.*, 2014].

Electron temperatures have a significant effect on peak electron densities, as was recognized by *Fox and Yeager* [2006]. They noted that altitude-dependent electron temperatures that increase with altitude through the ionospheric peak but do not vary with solar zenith angle could, due to associated changes in dissociative recombination rate coefficients, cause the exponent k to be less than 0.5, the maximum electron density to occur at a higher altitude than the maximum ion production rate, and the ionospheric peak to be relatively broad. We pursued these ideas with the one-dimensional Boston University Mars ionosphere model, specifically examining variations in simulated peak electron density with solar zenith angle [*Martinis et al.*, 2003, *Mendillo et al.*, 2004, 2011; *Lollo et al.*, 2012; *Matta et al.*, 2013]. Transport was suppressed in these simulations because transport processes do not affect plasma densities at the ionospheric peak. The incident solar irradiance, obtained from the SOLAR2000 model [*Tobiska et al.*, 2000; *Tobiska*, 2004; *Tobiska and Bouwer*, 2006], was attenuated as it passes through a neutral atmosphere of five species (O, CO_2, N_2, CO, and H_2) derived from the Mars Climate Database [*Forget et al.*, 1999; *Lewis et al.*, 1999]. Five ions, (O_2^+ , O^+, CO_2^+, N_2^+, and NO^+), were created by photoionization and secondary ionization. Secondary ionization by electron impact was parameterized as a wavelength-dependent ratio of secondary to primary ionization. We assumed that for each photon, each 28 eV of energy in excess of the ionization potential leads to another ionization event [*Lollo et al.*, 2012].

Two simulations were conducted, and electron temperatures were constant with time/solar zenith angle in each. In the first simulation, electron temperatures were prescribed to vary with altitude as in *Mendillo et al.* [2011], who adopted a representation based upon the available Viking observations. Here electron temperatures increased sharply from <200 K at 120 km to >1000 K at 180 km, a region that contains the main ionospheric peak. The resultant peak electron densities were proportional to 1/Ch raised to the power 0.37. This small exponent means that the simulated peak densities do not decrease with increasing solar zenith angle as rapidly as observed peak densities. Instead, as the peak altitude increases with increasing solar zenith angle, T_e at the peak also increases with increasing solar zenith angle. Consequently, the rate coefficient for plasma loss by dissociative recombination at the peak decreases with increasing solar zenith angle, which reduces the exponent. In the second simulation, electron temperatures were prescribed to be unphysically uniform with altitude at 120 K and the resultant peak electron densities were proportional to 1/Ch raised to the power 0.56, much closer to the observed value of 0.5.

This is paradoxical: a numerical simulation using electron temperatures that are consistent with the only available data completely fails to reproduce one of the most basic observed ionospheric trends, while a numerical simulation using unrealistic electron temperatures does much better. Clearly, the assumption of constant Viking-like electron temperatures throughout a sol is dubious, and not merely because the resultant exponent of 0.37 disagrees with observations. Based on this, we conclude that electron temperatures at

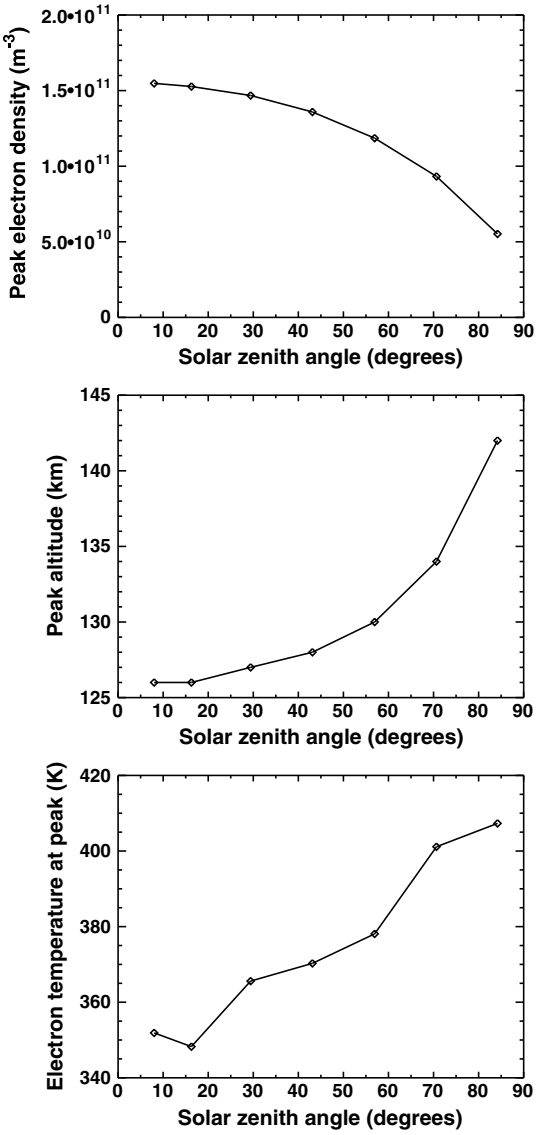

Figure 1. Conditions at the ionospheric peak from the model of *Matta et al.* [2014]. (top) Electron density. (middle) Altitude. (bottom) Electron temperature.

the main peak vary much less with solar zenith angle than is suggested by moving from the subsolar peak altitude of 120 km to the near-terminator peak altitude of 150 km on a Viking-based electron temperature profile.

One potential method for resolving this paradox is to consider both vertical and diurnal variations in energetics, as was done by *Matta et al.* [2014]. Figure 1 shows these predictions for how peak electron density, peak altitude, and electron temperature at the peak vary with solar zenith angle. No topside heating was applied in this application of the model. Electron temperatures at the peak vary surprisingly little with solar zenith angle, remaining within 15% of their mean. A fit of the predicted peak densities to $N_m \propto \mathrm{Ch}^{-k}$ yields a best fit k equal to 0.49, which is greater than the 0.37 obtained in the first simulation described above, which used altitude-dependent electron temperatures that were independent of solar zenith angle. This exponent of 0.49 is practically indistinguishable from the observed exponent k of 0.5. The transition from time static electron temperatures to time-varying electron temperatures has improved the agreement between the predicted exponent k (0.37 → 0.49) and the observed exponent k (0.5).

In the simulations of *Matta et al.* [2014], electron temperatures at fixed solar zenith angle increase with increasing altitude, electron temperatures at fixed altitude decrease with increasing solar zenith angle, and peak altitude increases with increasing solar zenith angle. It is not immediately obvious from *Matta et al.* [2014] why the net effect of these trends is that electron temperatures at the ionospheric peak increase with increasing solar zenith angle, rather than decrease. In order to develop an intuitive explanation for that behavior, we developed an analytic model of electron temperatures. Such a model is also useful for identifying the most important factors controlling electron temperatures near the ionospheric peak.

3. An Analytic Model of Electron Temperatures

A simplified analytic model of electron temperatures can be constructed to illustrate why electron temperatures at the ionospheric peak increase with increasing solar zenith angle and to connect their rate of increase to physical properties. We begin with the full versions of the energy and continuity equations used in the numerical simulations of *Matta et al.* [2014] and then neglect terms in order to reduce the situation to a tractable level of complexity. In essence, we set up versions of the continuity and energy equations, both of which contain N_e and T_e, and then eliminate N_e to obtain an expression for T_e.

The steady state continuity equation near the ionosphere peak, where photochemical equilibrium holds, is that the photoionization rate, P_e, equals the ion loss rate, L_e, which is αN_e^2. Here $\alpha = \gamma \left(T_e/T_r\right)^{-0.7}$, where

$\gamma = 2.4 \times 10^{-7}$ cm^3 s^{-1} and T_r is a reference temperature of 300 K [*Schunk and Nagy*, 2009]. Thus,

$$P_e = \gamma \left(T_e/T_r\right)^{-0.7} N_e^2 \tag{1}$$

Matta et al. [2014] evaluated the importance of the various terms in the energy equation and showed that solar heating and collisional cooling are the dominant terms in the electron energy equation around the ionospheric peak. Thus, in steady state, the solar heating rate, Q_e (power per unit volume), equals the collisional cooling rate, R_e. As a first approximation, Q_e can be parameterized as being proportional to the photoionization rate, P_e, such that $Q_e = \epsilon P_e$ [*Moore et al.*, 2008]. Although such an approximation is too simplified for precise work, it is suitable for back-of-the-envelope studies. In the simulations of *Matta et al.* [2014], dayside values of Q_e/P_e varied by only a factor of a few from one scale height below the main peak to five scale heights above. We adopt $\epsilon = 0.5$ eV, which is consistent with the simulations of *Matta et al.* [2014] near the altitude of peak production. The collisional cooling rate, R_e, due to rotational and vibrational interactions with CO_2 is $(5.8 + 3.35) \times 10^{-14} N_e n_n \left(T_e - T_n\right) T_e^{-0.5}$ [*Schunk and Nagy*, 2009; *Matta et al.*, 2014]. Here T_n and n_n are the neutral temperature and number density, respectively, and this expression yields R_e in units of eV cm^{-3} s^{-1} when N_e and n_n are in units of cm^{-3} and T_e and T_n are in units of Kelvin [*Matta et al.*, 2014]. This is equivalent to $R_e = \delta N_e n_n \left(\left(T_e - T_n\right)/T_r\right)\left(T_e/T_r\right)^{-0.5}$ where $\delta = 300^{0.5} \times 9.15 \times 10^{-14}$ eV cm^3 s^{-1} $= 1.6 \times 10^{-12}$ eV cm^3 s^{-1}. Thus,

$$\epsilon P_e = \delta N_e n_n \left(\left(T_e - T_n\right)/T_r\right)\left(T_e/T_r\right)^{-0.5} \tag{2}$$

Eliminating N_e between equations (1) and (2) gives

$$\left(\frac{T_e - T_n}{T_r}\right)^2 \left(\frac{T_e}{T_r}\right)^{-0.3} = \left(\frac{\epsilon^2 \gamma}{\delta^2}\right) \frac{P_e}{n_n^2} \tag{3}$$

We now express P_e and n_n in terms of altitude, z, in order to obtain a relationship between T_e and z. To do so, we assume that idealized Chapman theory is a useful description of the ionosphere of Mars. This assumption is not perfectly satisfied, but it serves as a reasonable starting place for our analytical investigation. No better analytical theory exists. Hence, $P_e = F_0 \exp\left(1 - x - \exp\left(-x\right)\right)/eH\mathrm{Ch}$ [*Chamberlain and Hunten*, 1987; *Withers* 2009]. Here $x = \left(z - z_{\mathrm{pp}}\right)/H$, where z_{pp}, the altitude of peak production, satisfies $\sigma H \mathrm{Ch} n_n\left(z_{\mathrm{pp}}\right) = 1$ and σ is the absorption/ionization cross section of the neutral species. Also, $n_n = \exp\left(-x\right)/\sigma H\mathrm{Ch}$. Substituting these expressions for P_e and n_n into equation (3), we obtain

$$\left(\frac{T_e - T_n}{T_r}\right)^2 \left(\frac{T_e}{T_r}\right)^{-0.3} = \left(\frac{\epsilon^2 \gamma F_0 \sigma^2 H\mathrm{Ch}}{\delta^2}\right) \exp\left(x - \exp\left(-x\right)\right) \tag{4}$$

This leads to

$$\theta^2 \left(1 + \theta\right)^{-0.3} = \left(\frac{T_n}{T_r}\right)^{-1.7} \left(\frac{\epsilon^2 \gamma F_0 \sigma^2 H}{\delta^2}\right) \mathrm{Ch} \exp\left(x - \exp\left(-x\right)\right) \tag{5}$$

$$\theta^2 \left(1 + \theta\right)^{-0.3} = w^2 \mathrm{Ch} \exp\left(x - \exp\left(-x\right)\right) \tag{6}$$

where $\theta = \left(T_e - T_n\right)/T_n$ and w is defined by equations (5) and (6). In order to estimate T_e, we adopt $F_0 = 10^{10}$ cm^{-2} s^{-1}, $\sigma = 3 \times 10^{-17}$ cm^2, $H = 10$ km, and $T_n = 181$ K [*Withers and Mendillo*, 2005]. This temperature is derived from the stated scale height using a CO_2-dominated atmosphere in which the acceleration due to gravity is 3.4 m s^{-2}. Together with the previously stated values for ϵ, δ, γ, and T_r, we obtain $w^2 = 0.5$. This value for w^2 sets the scale for differences between T_e and T_n. We also adopt a subsolar altitude of peak production, z_0, of 120 km so that $\sigma H n_n\left(z_0\right) = 120$ km.

$T_e\left(z, \chi\right)$ is shown in Figure 2 for altitudes at which the collisional cooling rate is greater than that of thermal conduction. Because the analytic model includes only the collisional cooling rate, we consider only altitudes where this term is the most significant cooling mechanism. Above this critical altitude, thermal conduction becomes an important cooling process [*Matta et al.*, 2014], which leads to near-isothermal conditions at high altitudes. The right-hand side of equation (6) increases rapidly with increasing altitude, due to the $\exp(x)$ term. As a result, predicted electron temperatures are unphysically large at high altitudes (tending toward infinity). The model becomes unrealistic above about 140 km.

Figure 2 also shows results from *Matta et al.* [2014]. Given the assumptions made in developing this analytic model, the agreement between the two sets of predictions is acceptable. The poor agreement at the lowest

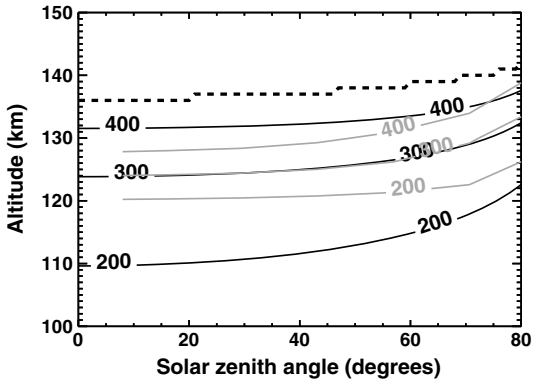

Figure 2. Dependence of predicted electron temperatures on solar zenith angle and altitude from the analytic model (solid black lines) and the results of *Matta et al.* [2014] (solid grey lines). No temperatures are plotted above the dashed line, which marks the critical altitude above which the analytic model is invalid.

altitudes is easily explained. At low altitudes, where the neutral atmosphere is relatively dense, electron temperatures very nearly equal neutral temperatures. This analytic model used an isothermal temperature of 181 K, whereas the work of *Matta et al.* [2014] used a temperature profile that varied from 130 K at 100 km to 180 K at 150 km. Hence, higher electron temperatures at low altitudes in the results of the analytic model reflect a warmer neutral atmosphere, rather than fundamental flaws in the analytic model.

It is clear that electron temperatures at the altitude of peak production, where $x = 0$, increase with increasing solar zenith angle since here $\theta^2 (1+\theta)^{-0.3} = w^2 \mathrm{Ch}/e$ (equation (6)). The prediction that $\theta^2 (1+\theta)^{-0.3}$ at the altitude of peak production is proportional to Ch, and the predicted value of the constant of proportionality can be tested by future observations (e.g., the Mars Atmosphere and Volatile EvolutioN (MAVEN) mission).

This analytic model provides an explanation for the prediction of *Matta et al.* [2014] that T_e at the peak increases as χ increases. In this model applied near the electron density peak, the electron collisional cooling rate, R_e, is proportional to the electron production rate, P_e, and R_e is proportional to $N_e n_n \left(T_e - T_n\right) T_e^{-0.5}$. At the peak, P_e and n_n are both proportional to 1/Ch. It follows that $N_e \left(T_e - T_n\right) T_e^{-0.5}$ at the peak is independent of solar zenith angle. Since $N_m \propto T_e^{0.35} \mathrm{Ch}^{-0.5}$, we have $\left(T_e - T_n\right) T_e^{-0.15} \propto \mathrm{Ch}^{0.5}$, which is consistent with equation (5). A best fit of the analytic model's electron densities at the altitude of peak production to the function $N_m \propto (\cos\chi)^{-k}$ yields a best fit exponent k of 0.43. This value is smaller than 0.5 due to the increase in T_e at the altitude of peak production with increasing χ. It appears that the analytic model has neglected some processes that in the real ionosphere make the exponent k closer to 0.5.

4. Conclusions

The model of *Matta et al.* [2014] has shown how electron temperatures depend on altitude and solar zenith angle, quantifying the expected increase in temperature with altitude at fixed solar zenith angle and the expected decrease in temperature with solar zenith angle at fixed altitude. It also predicts how electron temperatures at the ionospheric peak increase with solar zenith angle and that peak electron densities should be proportional to 1/Ch raised to the power 0.49, practically indistinguishable from the observed exponent k of 0.5.

The analytic model of electron temperatures predicts that the difference between electron and neutral temperatures is proportional to ϵ, the ratio of electron heating rate to electron production rate (neglecting the weakly varying $(1+\theta)^{-0.3}$ term in equation (5)). Its results provide an approach by which MAVEN observations of electron temperatures and other properties can constrain the ratio of electron heating rate to electron production rate. It is valid around and below the ionospheric peak, but the neglect of thermal conduction makes it invalid more than 1–2 scale heights above the ionospheric peak.

This analytic model also shows the functional dependence of electron temperatures on other influencing factors. The difference between electron and neutral temperatures is proportional to the square root of solar irradiance, which predicts how electron temperatures may change over the solar cycle and as solar irradiance varies on shorter timescales, such as the solar rotation period. In addition, the analytic model provides a functional description of how electron temperature increases with increasing altitude. Finally, this model provides an understandable explanation for why electron temperatures at the ionospheric peak increase, rather than decrease, with increasing solar zenith angle.

Acknowledgments
This work was supported, in part, by NASA awards NNX12AJ39G, NNX12AN80H, and NNX13AO35G. We thank Marina Galand, Luke Moore, and Michael Mendillo for their contributions to the modeling work that motivated this analytical study. Data presented in this manuscript can be produced either using the equations presented herein (results of analytic model) or as described in *Matta et al.* [2014] (results of numerical model).

The Editor thanks Niklas Edberg and an anonymous reviewer for their assistance in evaluating this paper.

References

Ågren, K., J.-E. Wahlund, P. Garnier, R. Modolo, J. Cui, M. Galand, and I. Müller-Wodarg (2009), On the ionospheric structure of Titan, *Planet. Space Sci.*, *57*, 1821–1827, doi:10.1016/j.pss.2009.04.012.

Bauer, S. J., and H. Lammer (2004), *Planetary Aeronomy*, Springer, New York.

Chamberlain, J. W., and D. M. Hunten (1987), *Theory of Planetary Atmospheres,* 2nd ed., Academic Press, New York.

Chapman, S. (1931a), The absorption and dissociative or ionizing effect of monochromatic radiation in an atmosphere on a rotating Earth, *Proc. Phys. Soc.*, *43*, 26–45.

Chapman, S. (1931b), The absorption and dissociative or ionizing effect of monochromatic radiation in an atmosphere on a rotating Earth. Part II. Grazing incidence, *Proc. Phys. Soc.*, *43*, 483–501.

Chen, R. H., T. E. Cravens, and A. F. Nagy (1978), The Martian ionosphere in light of the Viking observations, *J. Geophys. Res.*, *83*, 3871–3876.

Choi, Y. W., J. Kim, K. W. Min, A. F. Nagy, and K. I. Oyama (1998), Effect of the magnetic field on the energetics of Mars ionosphere, *Geophys. Res. Lett.*, *25*, 2753–2756, doi:10.1029/98GL51839.

Cravens, T. E., T. I. Gombosi, J. Kozyra, A. F. Nagy, L. H. Brace, and W. C. Knudsen (1980), Model calculations of the dayside ionosphere of Venus—Energetics, *J. Geophys. Res.*, *85*, 7778–7786, doi:10.1029/JA085iA13p07778.

Forget, F., F. Hourdin, R. Fournier, C. Hourdin, O. Talagrand, M. Collins, S. R. Lewis, P. L. Read, and J. Huot (1999), Improved general circulation models of the Martian atmosphere from the surface to above 80 km, *J. Geophys. Res.*, *104*, 24,155–24,176, doi:10.1029/1999JE001025.

Fox, J. L., and K. E. Yeager (2006), Morphology of the near-terminator Martian ionosphere: A comparison of models and data, *J. Geophys. Res.*, *111*, A10309, doi:10.1029/2006JA011697.

Fox, J. L., and K. E. Yeager (2009), MGS electron density profiles: Analysis of the peak magnitudes, *Icarus*, *200*, 468–479, doi:10.1016/j.icarus.2008.12.002.

Gurnett, D. A., et al. (2008), An overview of radar soundings of the martian ionosphere from the Mars Express spacecraft, *Adv. Space Res.*, *41*, 1335–1346, doi:10.1016/j.asr.2007.01.062.

Hanson, W. B., and G. P. Mantas (1988), Viking electron temperature measurements—Evidence for a magnetic field in the martian ionosphere, *J. Geophys. Res.*, *93*, 7538–7544.

Hantsch, M. H., and S. J. Bauer (1990), Solar control of the Mars ionosphere, *Planet. Space Sci.*, *38*, 539–542.

Johnson, R. E. (1978), Comment on ion and electron temperatures in the Martian upper atmosphere, *Geophys. Res. Lett.*, *5*, 989–992, doi:10.1029/GL005i011p00989.

Lewis, S. R., M. Collins, P. L. Read, F. Forget, F. Hourdin, R. Fournier, C. Hourdin, O. Talagrand, and J. Huot (1999), A climate database for Mars, *J. Geophys. Res.*, *104*, 24,177–24,194, doi:10.1029/1999JE001024.

Lollo, A., P. Withers, K. Fallows, Z. Girazian, M. Matta, and P. C. Chamberlin (2012), Numerical simulations of the ionosphere of Mars during a solar flare, *J. Geophys. Res.*, *117*, A05314, doi:10.1029/2011JA017399.

Martinis, C. R., J. K. Wilson, and M. J. Mendillo (2003), Modeling day-to-day ionospheric variability on Mars, *J. Geophys. Res.*, *108*(A10), 1383, doi:10.1029/2003JA009973.

Matta, M., P. Withers, and M. Mendillo (2013), The composition of Mars' topside ionosphere: Effects of hydrogen, *J. Geophys. Res. Space Physics*, *118*, 2681–2693, doi:10.1002/jgra.50104.

Matta, M., M. Galand, L. Moore, M. Mendillo, and P. Withers (2014), Numerical simulations of ion and electron temperatures in the ionosphere of Mars: Multiple ions and diurnal variations, *Icarus*, *227*, 78–88.

Mendillo, M., X. Pi, S. Smith, C. Martinis, J. Wilson, and D. Hinson (2004), Ionospheric effects upon a satellite navigation system at Mars, *Radio Sci.*, *39*, RS2028, doi:10.1029/2003RS002933.

Mendillo, M., A. Lollo, P. Withers, M. Matta, M. Pätzold, and S. Tellmann (2011), Modeling Mars' ionosphere with constraints from same-day observations by Mars Global Surveyor and Mars Express, *J. Geophys. Res.*, *116*, A11303, doi:10.1029/2011JA016865.

Moore, L., M. Galand, I. Mueller-Wodarg, R. Yelle, and M. Mendillo (2008), Plasma temperatures in Saturn's ionosphere, *J. Geophys. Res.*, *113*, A10306, doi:10.1029/2008JA013373.

Morgan, D. D., D. A. Gurnett, D. L. Kirchner, J. L. Fox, E. Nielsen, and J. J. Plaut (2008), Variation of the Martian ionospheric electron density from Mars Express radar soundings, *J. Geophys. Res.*, *113*, A09303, doi:10.1029/2008JA013313.

Nielsen, E., H. Zou, D. A. Gurnett, D. L. Kirchner, D. D. Morgan, R. Huff, R. Orosei, A. Safaeinili, J. J. Plaut, and G. Picardi (2006), Observations of vertical reflections from the topside Martian ionosphere, *Space Sci. Rev.*, *126*, 373–388, doi:10.1007/s11214-006-9113-y.

Němec, F., D. D. Morgan, D. A. Gurnett, F. Duru, and V. Truhlík (2011), Dayside ionosphere of Mars: Empirical model based on data from the MARSIS instrument, *J. Geophys. Res.*, *116*, E07003, doi:10.1029/2010JE003789.

Rohrbaugh, R. P., J. S. Nisbet, E. Bleuler, and J. R. Herman (1979), The effect of energetically produced O_2^+ on the ion temperatures of the Martian thermosphere, *J. Geophys. Res.*, *84*, 3327–3338, doi:10.1029/JA084iA07p03327.

Safaeinili, A., W. Kofman, J. Mouginot, Y. Gim, A. Herique, A. B. Ivanov, J. J. Plaut, and G. Picardi (2007), Estimation of the total electron content of the martian ionosphere using radar sounder surface echoes, *Geophys. Res. Lett.*, *34*, L23204, doi:10.1029/2007GL032154.

Schunk, R. W., and A. F. Nagy (2009), *Ionospheres,* 2nd ed., Cambridge Univ. Press, New York.

Singhal, R. P., and R. C. Whitten (1988), Thermal structure of the ionosphere of Mars—Simulations with one- and two-dimensional models, *Icarus*, *74*, 357–364, doi:10.1016/0019-1035(88)90048-6.

Tobiska, W. K. (2004), SOLAR2000 irradiances for climate change research, aeronomy and space system engineering, *Adv. Space Res.*, *34*, 1736–1746, doi:10.1016/j.asr.2003.06.032.

Tobiska, W. K., and S. D. Bouwer (2006), New developments in SOLAR2000 for space research and operations, *Adv. Space Res.*, *37*, 347–358, doi:10.1016/j.asr.2005.08.015.

Tobiska, W. K., T. Woods, F. Eparvier, R. Vierreck, L. Floyd, D. Bouwer, G. Rottman, and O. R. White (2000), The SOLAR2000 empirical solar irradiance model and forecast tool, *J. Atmos. Sol. Terr. Phys.*, *62*, 1233–1250.

Withers, P. (2009), A review of observed variability in the dayside ionosphere of Mars, *Adv. Space Res.*, *44*, 277–307, doi:10.1016/j.asr.2009.04.027.

Withers, P., and M. Mendillo (2005), Response of peak electron densities in the martian ionosphere to day-to-day changes in solar flux due to solar rotation, *Planet. Space Sci.*, *53*, 1401–1418, doi:10.1016/j.pss.2005.07.010.